Estimate Vibration Risk for Relief and Process Piping

July 17, 2012

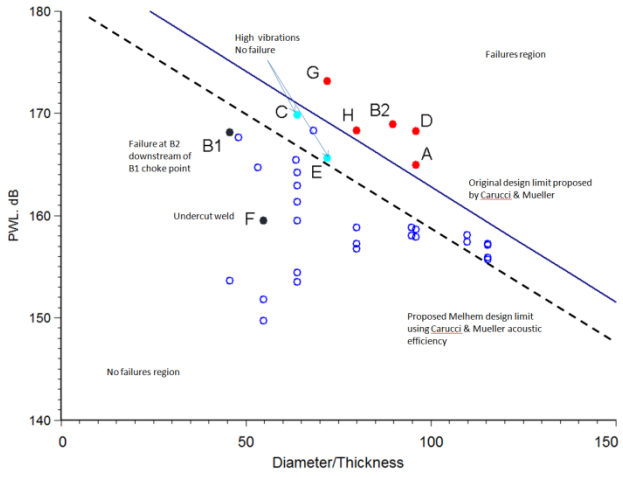

Notice:

This report was prepared by ioMosaic for public disclosure. This report represents ioMosaic's best judgment in light of information made available to us. Opinions in this report are based in part upon data and information obtained from the open literature. The reader is advised that ioMosaic has not independently verified the data or the information contained therein. This report must be read in its entirety. The reader understands that no assurances can be made that all liabilities have been identified. This report does not constitute a legal opinion.

No person has been authorized by ioMosaic to provide any information or make any representations not contained in this report. Any use the reader makes of this report, or any reliance upon or decisions to be made based upon this report are the responsibility of the reader. ioMosaic does not accept any responsibility for damages, if any, suffered by the reader based upon this report.

ioMosaic Corporation
93 Stiles Road
Salem, New Hampshire
03079 U.S.A.

Contents

List of Tables

List of Figures

Estimate Vibration Risk for Relief and Process Piping

G. A. MELHEM
ioMosaic Corporation
93 Stiles Road
Salem, New Hampshire 03079

1 Introduction

Fatigue failure of relief and/or process piping caused by vibration can develop due to the conversion of flow mechanical energy to noise. Factors that have led to an increasing incidence of noise vibration related fatigue failures in piping systems include but are not limited to (a) increasing flow rates as a result of debottlenecking which contributes to higher flow velocities with a correspondingly greater level of turbulent energy, (b) frequent use of thin-walled piping which results in higher stress concentrations, particularly at small bore and branch connections, (c) design of process piping systems on the basis of a static analysis with little attention paid to vibration induced fatigue, (e) and lack of emphasis of the issue of vibration in piping design codes. Piping vibration is often considered on an ad-hoc or reactive basis. According to the UK Health and Safety Executive (HSE), 21 % of all piping failures offshore are caused by fatigue/vibration. Typical systems at risk include large compressor recycle systems and high capacity pressure relief depressuring systems. For relief and flare piping, flow induced turbulence and high frequency acoustic excitations are key concerns.

2 Flow Induced Turbulence

Fluid flow in pipes generates turbulent energy (pressure fluctuations). Dominant sources of turbulence are associated with flow discontinuities in the piping systems (e.g., partially closed valves, short radius, mitered bends, tees or expanders). The level of turbulence intensity is a function of pipe size, fluid density, viscosity, velocity, and structural support. High noise levels are generated by high velocity fluid impingement on the pipe wall, turbulent mixing, and if the flow is choked, shock waves downstream of flow restriction, which leads to high frequency excitation/vibration.

3 High Frequency Excitation

High frequency acoustic energy is often generated by a pressure reducing device such as a relief valve, control valve, or orifice plate. Acoustic induced piping failure is of a particular concern for safety related systems (e.g. relief and blowdown/depressuring). The severity of high frequency

acoustic excitation is primarily a function of the pressure upstream and downstream of the pressure reducing device, pipe diameter, and the fluid volumetric flow. Acoustically induced piping failures are known to occur at non-asymmetric discontinuities in the downstream piping such as small bore and branch connections and welded supports.

4 Additional Causes of Vibration

Additional causes of piping vibration include mechanical excitation, pulsation, vortex shedding, surge or momentum changes associated with valves, cavitation, and flashing. Mechanical excitations are often associated with pipes connected with reciprocating compressors, pumps, or rotating machinery. Such connection machines cause vibration of the pipe and its support structure. Thermowells are intrusive fittings and are subject to static and dynamic fluid forces. Vortex shedding is the dominant concern as it is capable of forcing the thermowell into flow-induced resonance and consequent fatigue failure. The latter is particularly significant at high fluid velocities.

5 Relief and Depressuring Systems

Depressuring systems are often subjected to acoustic energy (rapidly fluctuating pressure forces) generated by flow turbulence which is accentuated by flow restricting devices within the flow path. The magnitude of pressure fluctuations depends on the mass flow rate, speed of sound, and density. For choked flow, intense noise due to large shock discontinuities and pressure fluctuations is generated. The generated noise is non-periodic due to the randomness of the pressure fluctuations. Choked flow typically leads to a wide frequency spectrum with peak values than can exceed 1000 Hz. Vibrations associated with small fittings and branch connections are of special concern because they introduce discontinuities and stress concentration points.

In many situations resonance can onset which can lead to magnification of static piping loads up to a factor of 50 times. The presence of discontinuities such as tees and welded pipe supports can further increase these loads.

6 Noise Generation

A pressure reducing device or relief device controls flow by converting internal energy into kinetic energy. Some energy is converted to heat through friction (viscous forces) by intense turbulence and shock formation. Some of the energy is also transferred to the pipe wall as vibration, and a portion of this is radiated as noise. The primary noise generating mechanism is the confined jet of fluid formed between the upstream and downstream locations. Flow noise can be modeled as noise of a confined jet. As a result, the noise-generation mechanisms are turbulent mixing, turbulence boundary interaction, shock, shock/turbulence interaction and flow separation.

Since the noise is generated downstream of a flow restriction, most of the acoustic energy is ra-

diated to the downstream piping, which becomes the transmitting medium. As the noise travels downstream along the inside of the pipe in the fluid it radiates through the pipe wall along its entire length.

7 How to Calculate Sound Power Level

We can calculate the sound power level in a fundamental way by assigning an efficiency factor to provide the fraction of flow mechanical energy that is converted to noise:

$$W = \eta \frac{1}{2} \dot{m} u^2 \tag{1}$$

$$L_W = 10 \log_{10} \left[\frac{W}{10^{-12}} \right] = 10 \log_{10} W + 120 = 10 \log_{10} \left[\eta \frac{1}{2} \dot{m} u^2 \right] + 120 \tag{2}$$

where W is the flow mechanical power or energy, L_W is the sound power level in dB, and η is defined as the acoustical efficiency factor. If the flow is choked, then W becomes:

$$W = \eta \frac{1}{2} \dot{m} u_{sonic}^2 \tag{3}$$

If a value of η can be estimated for single and multi-phase flow, then the sound power level can be easily calculated not only for pressure reducing devices but also for pipe flow. Attenuation due to friction and temperature changes can be calculated from pipe flow equations in a more detailed manner. Computer codes such as SuperChems can then calculate the sound power level at every axial location for flow piping for single and multi-phase flow.

For incompressible flow, the value of flow velocity for an ideal nozzle can be calculated from the mechanical energy balance:

$$u = \sqrt{\frac{2}{\rho_l} \Delta P} \tag{4}$$

Substituting the above equation for u in Equation 1 yields the following Equation for W for liquid flow through an ideal nozzle:

$$W = \eta \dot{m} \frac{\Delta P}{\rho_l} \tag{5}$$

For liquid flow, a typical value of η is approximately 10^{-8}.

All gas flow acoustic efficiencies have been reported to approach 1 % of the total flow mechanical energy for rockets [4]. This is illustrated in Figure 1. When the acoustic efficiency is plotted against the flow mechanical power Figure 1 is obtained. The measured curve indicates that the acoustic efficiency falls off as the flow mechanical energy gets larger while the calculated curve [5] indicates increasing acoustic efficiencies.

Figure 1: Acoustic Efficiency Trends

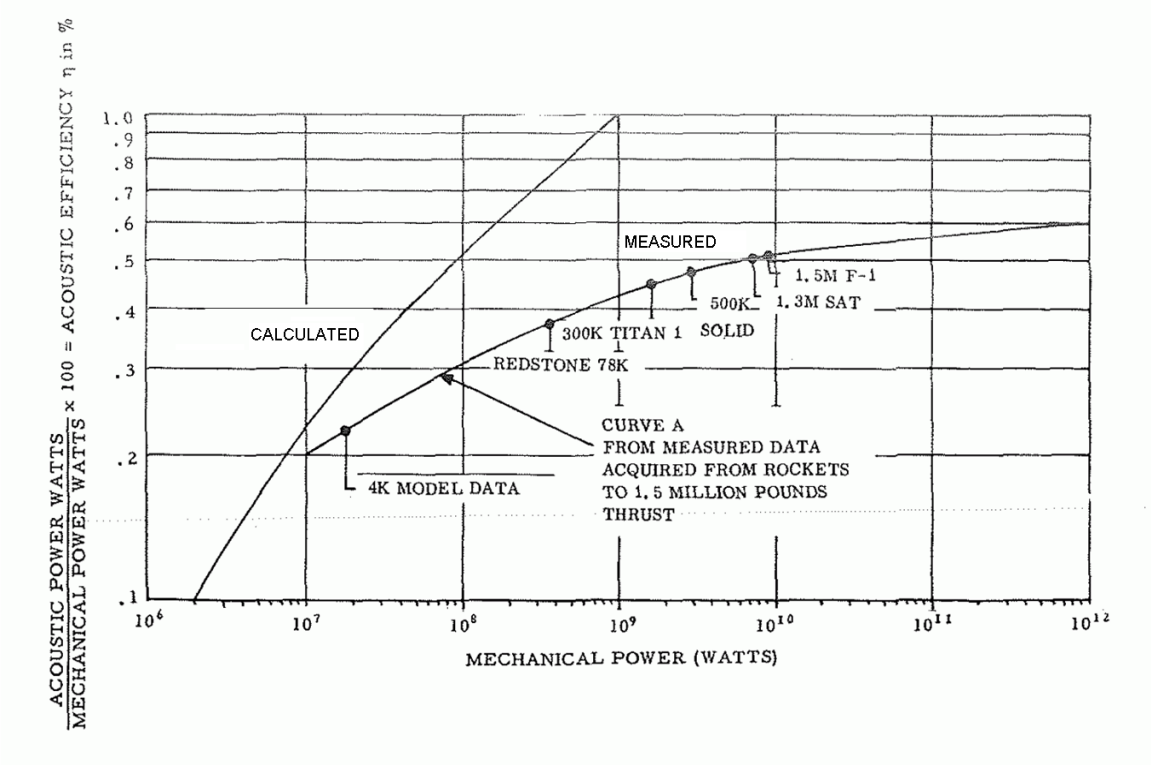

Two-phase flow sound power level can also be calculated using Equation 1. Recent work by Singh et al. ([6], [7]) demonstrated that more attenuation of noise is exhibited by two-phase flow. Therefore, using the gas acoustic efficiency values will overpredict sound power and noise levels for two-phase flow.

8 Existing Methods and Guidance

Current API, AIChE/CCPS, and AIChE/DIERS pressure relief and flare systems guidelines and standards do not formally address vibration risk. They do not offer specific guidance on velocity limitations other than backpressure calculations and they do not offer guidance on acoustic induced or turbulence induced piping vibration fatigue failure. The Marine Technology Directorate Limited (MTD) has published in 1999 "Guidelines for the Avoidance of Vibration Induced Fatigue in Process Pipework" [8]. A second edition of these guidelines were published in 2008 by the Energy Institute [9]. The methods outlined in these guides have been incorporated in the SuperChems Expert ioVIPER modules. The MTD/Energy Institute guidelines provide qualitative and quantitative methods for the assessment of piping vibration failure risk and depending on the calculated risk level they provide generic guidance for the mitigation of vibration risk.

Many operating companies have established their own internal guidance for evaluating and minimizing piping vibration risk. Although these criteria vary from company to company, they all in

general include a limit of flow velocity in some form.

A common criteria used in relief systems is to limit the value of flow Mach number to a limiting value ranging from 0.3 to 0.9:

$$0.3 \leq M = \frac{u}{u_{sonic}} \leq 0.9 \tag{6}$$

Another common criteria often encountered is to limit the dynamic pressure component or kinetic energy of a flow stream to a value of 100,000 Pascals for gas flow:

$$\rho u^2 \leq 1 \times 10^5 \ \ \mathrm{kg/m/s^2} \tag{7}$$

and 50,000 for two-phase flow:

$$\rho u^2 \leq \frac{1}{2} \times 10^5 \ \ \mathrm{kg/m/s^2} \tag{8}$$

The 2006 fifth edition of the NORSOK Process Design Standard P-001 limits the flow velocities for all flare lines to $\rho u^2 \leq 200000 \ \mathrm{kg/m/s^2}$ for single and multiphase flow. The piping for flare headers and sub-headers are designed for a maximum Mach number of 0.6 and lines downstream of pressure relief valves to the first sub-header are designed for a maximum Mach number of 0.7. For process lines the maximum design velocity for gas pipes is limited to 60 $\mathrm{m/s}$ or $u \leq 175 \frac{1}{\rho^{0.43}}$ whichever is less. The maximum velocity for two-phase lines is limited to $u \leq 183 \frac{1}{\rho^{0.5}}$ or:

$$\rho u^2 \leq 183^2 \leq 33489 \ \ \mathrm{kg/m/s^2} \tag{9}$$

9 The Method of Carucci and Mueller

Carucci and Mueller have published guidance for the estimation of sound power levels for control valves and pressure reducing devices (see [10] and [11]).

$$\begin{aligned} L_W &= 10 \times \log_{10} \left[\left(\frac{P_1 - P_2}{P_1} \right)^{3.6} \times \dot{m}^2 \times \left(\frac{T_1}{M_w} \right)^{1.2} \right] + 126.1 & (10) \\ &= 10 \times \log_{10} \left[4 \times \left(\frac{P_1 - P_2}{P_1} \right)^{3.6} \times \dot{m}^2 \times \left(\frac{T_1}{M_w} \right)^{1.2} \right] + 120 & (11) \\ &= 36 \log_{10} \left(\frac{P_1 - P_2}{P_1} \right) + 20 \log_{10} (\dot{m}) + 12 \log_{10} \left(\frac{T_1}{M_w} \right) + 126.1 & (12) \end{aligned}$$

where P_1 is the upstream pressure or source pressure, P_2 is the downstream pressure, T_1 is the source temperature, $\dot{m}$ is the mass flow rate, and M_w is the molecular weight. Attenuation of noise due to friction and heat conduction losses is estimated from the following equation:

$$L_{W,At} = 0.06 \frac{L}{D_i} \tag{13}$$

where L is the pipe length and D_i is the internal pipe diameter. For an L/D of 50 the attenuation loss is 3 dB. Abrupt changes in flow area (expansion) in the piping can also lead to attenuation. The decrease in sound power level can be estimated from the following equation:

$$L_{W,Ex} = 2\left(\frac{D_2}{D_1} - 1\right) \tag{14}$$

where $D_2 > D_1$. A 3 dB reduction is typically applied to the flow leaving a tee in each direction or entering into header or a large drum or vessel. The Carucci and Mueller Equation 12 is used by the Energy Institute Guidelines for the assessment of failure likelihood for high frequency acoustic excitation (see Pages 59-62 in [9]). Note that the Carucci and Mueller equation cannot be easily applied to complex piping systems, multi-phase systems, and relief piping with multiple chokes. Some companies also add 6 dB to the sound power level estimate when sonic flow exists at a branch connection to account for amplified dynamic strain response.

9.1 Analysis of the Carucci and Mueller Data Set

Careful analysis of the Carucci and Mueller data set (see Table 1) indicates that the source pressures were high enough to produce choked (sonic) flow through a flow limiting orifice or valve upstream of the failure point further downstream, often at a branch or line connection. This important point was missed by Eisinger who used the downstream (non-choked) flow velocity to establish his Mach number based failure criterion. We were also able to reproduce Eisinger's estimates of the original Caruci and Mueller data set based on his published paper.

Carucci and Mueller provided enough data in their original paper to allow the calculation of the upstream flow limiting flow area and choke point conditions (this is possible because they reported the actual flow rates) as well as the conditions downstream of the flow limiting device in the discharge piping. Note that the sound power level estimate upstream of the choke points should be based on the pressure difference (or pressure ratio) of the source pressure and the choke point. The sound pressure level downstream of the choke point (the primary cause of acoustic induced fatigue failure in downstream piping of the choked point) should be based on the difference (or pressure ratio) of the choke point and the shock discontinuity pressure downstream of the choke point. The original equation proposed by Carucci and Mueller used the pressure difference (or ratio) between the source pressure and the exit pressure downstream of the choke point. This yields an overestimate of the sound pressure. This overestimate is somewhat tempered by the fact that the pressure difference ratio to the source pressure is raised to the 3.6 power.

The following information was provided by Carucci and Mueller regarding the five failures and two high vibrations cases observed in Table 1:

A Failure occurred during startup. Sonic velocity is achieved at the 6 inch branch connection of a 24 inch pipe run downstream of the recycle valve. The sound power level estimate considers the combined acoustic energy generated by the letdown valve and the sonic condition at the branch connection. Upstream pressure at branch connection estimated to be 98.8 psia.

Table 1: Vibration Risk Data Set used by Carucci and Mueller and reproduced by Melhem

CASE	SERVICE	T1. K	P1. bara	T2. K	P2. bara	D2. m	u2. m/s	Exit Mach Number, M2	Mass Flow Rate, kg/s	Heat Capcity Ratio, Cp/Cv	Restriction Orifice / Valve Flow Speed. m/s	Carucci and Mueller Acoustic Efficiency. %	IEC Acoustic Efficiency. %	PWL_cm. dB	PWL_mel. dB	PWL_cm - PWL_mel. dB	PWL_mel (IEC). dB
A	Propylene Compressor Recycle	319.26	20.55	238.91	1.59	0.610	32.50	0.137	29.74	1.13	224.30	0.65	0.85	168.5	165.0	3.5	161.5
B1	Natural Gas Pressure	318.71	42.75	226.00	6.27	0.254	125.60	0.399	48.26	1.22	322.99	2.54	0.91	170.9	168.1	2.8	163.6
B2	Natural Gas Letdown to Flare	318.71	5.17	270.38	2.07	0.711	58.20	0.169	48.26	1.22	357.00	0.41	0.69	171.4	168.9	2.5	163.3
C	Natural Gas Letdown to Flare	308.15	47.57	195.68	4.14	0.406	64.40	0.218	47.63	1.23	311.29	4.17	0.95	171.8	169.8	2.0	163.4
D	Nitrogen Compressor Recycle	310.93	6.96	280.31	3.72	0.610	93.80	0.297	119.70	1.20	324.76	1.05	0.79	168.3	168.2	0.1	167.0
E	Nitrogen Compressor Recycle	310.93	16.82	267.59	7.03	0.457	60.10	0.194	84.80	1.21	328.35	0.79	0.66	168.8	165.6	3.3	164.8
F	Natural Gas Compressor Recycle	330.37	51.09	220.53	13.86	0.305	28.80	0.093	35.28	1.45	272.52	0.69	0.82	164.9	159.5	5.4	160.3
G	Desuperheater Steam	802.59	99.97	480.32	10.34	0.457	49.80	0.093	36.89	1.29	619.65	2.91	0.94	175.5	173.1	2.4	168.2
H	Desuperheater Steam	658.15	43.09	476.11	10.34	0.508	49.60	0.093	45.99	1.29	586.00	0.86	0.83	163.9	168.3	-4.4	168.9
1	Process Gas Compressor Recycle	308.15	13.17	204.98	1.03	0.406	122.80	0.461	27.09	1.19	296.81	2.22	0.95	165.9	164.2	1.7	160.6
2	Process Gas Compressor Recycle	311.48	38.75	265.88	10.00	0.305	14.20	0.048	13.86	1.13	258.54	0.32	0.83	156.6	151.8	4.8	155.9
3	Propylene Compressor Recycle	316.48	20.55	262.14	3.24	0.406	15.70	0.065	12.60	1.11	209.52	0.81	0.91	156.0	153.5	2.5	154.0
4	Process Gas Compressor Recycle	300.37	2.48	257.91	1.03	0.508	145.60	0.450	34.78	1.21	325.00	0.26	0.77	161.3	156.7	4.6	161.5
5	Process Gas Compressor Recycle	310.93	15.86	215.12	2.21	0.406	68.70	0.226	25.33	1.23	357.01	1.21	0.91	165.2	162.9	2.3	161.7
6	Process Gas Compressor Recycle	300.93	39.44	250.67	15.51	0.254	26.10	0.075	20.66	1.24	330.10	0.20	0.78	158.3	153.6	4.7	159.4
7	Propylene Compressor Recycle	310.93	16.69	233.88	1.38	0.356	131.30	0.575	38.05	1.13	216.35	3.92	0.95	166.6	165.4	1.2	159.3
8	Propylene Compressor Recycle	310.93	16.69	234.72	1.38	0.508	59.20	0.259	35.03	1.13	216.35	3.61	0.95	165.9	164.7	1.2	158.9
9	Waste Steam Dump	403.71	2.76	370.82	1.03	0.406	245.10	0.566	18.90	1.10	436.60	0.15	0.77	160.5	154.4	6.1	161.4
10	Process Gas Compressor Recycle	302.59	10.69	207.90	1.03	0.406	95.80	0.357	20.92	1.19	295.15	1.49	0.94	163.2	161.3	1.9	159.3
11	Process Gas Compressor Recycle	308.15	54.81	263.43	27.51	0.305	7.20	0.016	9.15	1.29	441.77	0.10	0.79	150.5	149.7	0.8	158.5
12	Natural Gas Compressor Recycle	308.15	3.79	282.54	2.48	0.914	28.40	0.075	39.69	1.26	315.99	0.19	0.73	155.4	155.7	-0.3	161.6
13	Natural Gas Compressor Recycle	308.15	6.48	279.42	4.00	0.914	17.30	0.046	39.44	1.25	334.77	0.24	0.75	157.2	157.2	0.0	162.2
14	Natural Gas Compressor Recycle	308.15	11.45	282.82	6.76	0.762	14.40	0.039	38.93	1.19	346.05	0.28	0.76	158.1	158.1	0.0	162.5
15	Natural Gas Compressor Recycle	308.15	21.79	266.72	11.65	0.660	10.10	0.027	36.04	1.30	359.11	0.33	0.78	159.4	158.8	0.6	162.6
16	Natural Gas Compressor Recycle	308.15	40.75	272.56	21.99	0.610	6.30	0.017	35.91	1.25	344.77	0.34	0.78	159.2	158.6	0.6	162.2
17	Natural Gas Compressor Recycle	308.15	80.12	271.44	40.89	0.508	4.80	0.013	35.41	1.23	324.89	0.40	0.78	160.1	158.8	1.3	161.6
18	Natural Gas Compressor Recycle	308.15	172.99	240.53	79.98	0.406	3.80	0.010	35.41	1.47	326.41	0.71	0.82	161.5	161.3	0.2	161.9
19	Natural Gas Compressor Recycle	308.15	3.86	280.10	2.34	0.914	27.60	0.074	37.17	1.24	340.74	0.24	0.75	157.3	157.1	0.2	162.1
20	Natural Gas Compressor Recycle	308.15	6.21	281.91	3.93	0.914	16.50	0.044	36.79	1.24	325.37	0.20	0.74	155.9	155.9	0.0	161.6
21	Natural Gas Compressor Recycle	308.15	10.62	274.09	6.27	0.762	14.30	0.038	36.04	1.29	345.37	0.26	0.76	157.4	157.4	0.0	162.1
22	Natural Gas Compressor Recycle	308.15	19.72	266.35	10.62	0.660	10.10	0.027	33.01	1.31	359.23	0.30	0.78	158.4	158.0	0.4	162.2
23	Natural Gas Compressor Recycle	308.15	36.82	263.14	19.79	0.610	6.40	0.017	32.89	1.34	346.54	0.31	0.78	158.4	157.9	0.5	161.9
24	Natural Gas Compressor Recycle	308.15	64.47	270.22	36.96	0.508	4.90	0.013	32.82	1.31	319.94	0.32	0.77	157.3	157.2	0.1	161.1
25	Natural Gas Compressor Recycle	308.15	139.48	320.30	64.54	0.406	4.20	0.012	32.76	0.95	311.67	0.56	0.80	160.7	159.5	1.2	161.1
26	Propane Compressor Recycle	308.15	12.07	234.24	0.97	0.457	143.50	0.644	50.40	1.12	217.76	4.82	0.96	168.9	167.6	1.3	160.6
27	Steam Desuperheater	658.15	43.09	522.78	10.34	0.762	22.00	0.041	45.99	1.19	564.55	0.91	0.83	161.2	168.3	-7.1	167.9

B1/B2 This system consisted of a control valve letting down pressure to a safety valve / flare header system. The failure occurred after five to ten hours of operation as a crack at a 10 inch branch connection to 28 inch header. Sonic velocity was achieved at both the control valve and the 10 inch branch connection to the 28 inch flare header. As such, two pertinent data points are established:

1. Acoustic energy within 10 inch line as generated by valve (not the failure point), and
2. Combined acoustic energy within 28 in header as generated by valve and sonic condition at the 10 in branch connection (the failure point).

C High vibrations, no failures.

D Failure during startup. Cracks were observed in a 24 inch line downstream of the compressor recycle valve after twelve hours of operation. The cracks were near the branch connections of a 6 inch line and a 3/4 inch drain valve and at an I-beam support welded to the pipe at the elbow immediately downstream of the control valve.

E High vibration, no failures.

F Failure at severely undercut weld on 300 mm (12 in.) line made to fasten conduit support Clip. Points of high stress concentration later eliminated.

G This system consisted of six, parallel, high pressure steam letdown valves, each with a downstream, three pass contra-flow attemporator and an in-line silencer. Failure of the 18 inch attemporator shells occurred after four hundred hours of operation.

H This system included four parallel desuperheaters located downstream of control valves. Several cracks developed in this system after two to three months of operation. Two to three of the four letdown valves were discharging steam through a 10 inch connection to a 20 inch header which swaged up to a 30 inch diameter. Longitudinal cracking occurred at the bottom of the 20 inch header at a transverse guide 0.5 meters downstream of the fourth 10 inch branch connection. In addition, a 1 inch bypass line for a block valve downstream of the third letdown valve cracked and the 20 inch header cracked around a pressure tap downstream of the transverse guide.

Table 1 compares the acoustic efficiencies implied in the Carucci and Mueller method (at the upstream choke point) vs. acoustic efficiencies established using IEC methods described later on in this paper. The acoustic efficiencies implied by the Carucci and Mueller method at the upstream choke point ranged from 0.1 to 5 percent while the IEC acoustic efficiency ranged from 0.67 to 1 percent. The Carucci and Mueller method is based on acoustic energy theories encompassing both jet and choked flow noise as well as test data from work performed by Exxon research and engineering. As discussed in later sections, the experience based failure criteria originally developed by Carucci and Mueller can only be used with sound power levels calculated by Equation 12.

The implied acoustic efficiency by Equation 12 is proportional to the mass flow rate and inversely proportional to u^2:

$$\eta = 8\left(1 - \frac{P_2}{P_1}\right)^{3.6}\left(\frac{T_1}{M_w}\right)^{1.2}\left(\frac{\dot{m}}{u^2}\right) \tag{15}$$

If we consider the case of an ideal gas undergoing isentropic choked (sonic) flow through a restriction orifice, we can establish the following expressions for variables of interest at the choke point:

$$T_2 = 2\frac{T_1}{\gamma+1} \tag{16}$$

$$P_2 = P_1\left(\frac{2}{\gamma+1}\right)^{\frac{\gamma}{\gamma-1}} \tag{17}$$

$$\rho_2 = \frac{P_2 M_w}{R_g T_2} \tag{18}$$

$$u_2 = \sqrt{\frac{\gamma R_g T_2}{M_w}} \tag{19}$$

$$\dot{m} = \rho_2 u_2 A_o \tag{20}$$

Substituting the values of mass flow rate $\dot{m}$, choked flow velocity u_2, and choke pressure P_2 in Equation 15, we obtain the following simplified expression for the Carucci and Mueller acoustic efficiency after some algebraic manipulations:

$$\eta = (4.7950\gamma - 2.5882)\left(\frac{M_w}{T_1}\right)^{0.3} P_1 A_o \tag{21}$$

Where A_o is the effective restriction orifice flow area in m^2, P_1 is the upstream pressure in bara, T_1 is the upstream temperature in Kelvin, and η is the calculated Carucci and Mueller acoustic efficiency in percent. This expression shows that the Carucci and Mueller acoustic efficiency is directly proportional to upstream pressure, and the restriction orifice flow area (flow rate). It can be shown that the Carucci and Mueller acoustic efficiency produces unrealistic values for high pressure systems, large flow area, and/or mixtures with high molecular weights.

If we consider the case of methane discharging through a restriction with an effective flow area of $0.1\ \mathrm{m}^2$, upstream temperature of $373.15\ \mathrm{K}$, and an upstream pressure of $100\ \mathrm{bara}$, the calculated acoustic efficiency is:

$$\eta = (4.7950 \times 1.282 - 2.5882)\left(\frac{16}{373.15}\right)^{0.3} \times 100 \times 0.1 \tag{22}$$

$$= 3.559 \times 0.388 \times 100 \times 0.1 = 13.8\% \tag{23}$$

The same value can also be calculated by calculating $\dot{m}$, u_2, P_2, and η directly from the above ideal gas flow equations and Equation 15:

$$T_2 = 2\frac{T_1}{\gamma+1} = 2\frac{373.15}{1.282+1} = 327.05\ \mathrm{K} \tag{24}$$

$$P_2 = P_1\left(\frac{2}{\gamma+1}\right)^{\frac{\gamma}{\gamma-1}} = 100\left(\frac{2}{1.282+1}\right)^{\frac{1.282}{1.282-1}} = 54.9\ \mathrm{bara} \tag{25}$$

$$\rho_2 = \frac{P_2 M_w}{R_g T_2} = \frac{54.9 \times 100000 \times 16}{8314 \times 327.03} = 32.306 \text{ kg/m}^3 \quad (26)$$

$$u_2 = \sqrt{\frac{\gamma R_g T_2}{M_w}} = \sqrt{\frac{1.282 \times 8314 \times 327.03}{16}} = 466.76 \text{ m/s} \quad (27)$$

$$\dot{m} = \rho_2 u_2 A_o = 32.306 \times 466.76 \times 0.1 = 1507.63 \text{ kg/s} \quad (28)$$

$$\eta = 8\left(1 - \frac{P_2}{P_1}\right)^{3.6}\left(\frac{T_1}{M_w}\right)^{1.2}\left(\frac{\dot{m}}{u^2}\right) \quad (29)$$

$$= 8 \times (1 - 0.549)^{3.6} \times \left(\frac{373.15}{16}\right)^{1.2} \times \left(\frac{1507.63}{466.76^2}\right) \quad (30)$$

$$= 8 \times 0.0568 \times 43.78 \times 69.2 \times 10^{-4} \quad (31)$$

$$= 0.1376 \text{ or } 13.76\% \quad (32)$$

A similar equation to 21 can be derived for the acoustic efficiency downstream of the choke point:

$$\eta = (68.63 - 4.836\gamma)\left[1 - (1.0397 + 0.6096\gamma)\frac{P_b}{P_1}\right]^{3.6}\left(\frac{M_w}{T_1}\right)^{0.3} P_1 A_o \quad (33)$$

where P_b is the superimposed backpressure downstream of the choke point. Applying Equation 33 to the same example above we calculate an acoustic efficiency of 227 percent at a backpressure of 1 bara:

$$\eta = (68.63 - 4.836 \times 1.282)\left[1 - (1.0397 + 0.6096 \times 1.282)\frac{1}{100}\right]^{3.6}\left(\frac{16}{375}\right)^{0.3} \times 100 \times 0.1$$

$$= 62.430 \times 0.9359 \times 0.388 \times 100 \times 0.1$$

$$= 226.70\% \quad (34)$$

It is evident from the actual data reported by Carucci and Mueller and from the above theoretical proof that the acoustic efficiency used by Carucci and Mueller in their equation can produce unrealistic values, well in excess of 1 percent. Thus, it is recommended that the Carucci and Mueller acoustic efficiency value be limited to a maximum of 2 percent if the calculated value exceeds 2 percent.

10 Failure Criteria

Several methods are now available for screening and analyzing the potential failure risk of piping caused by vibration. These methods include:

- Experience Based - D/t method or D Method
- Experience Based - Mach number method (Not recommended)
- MTD methods

- Detailed structural dynamics methods

The experience based methods center around correlating likelihood of failure based on actual experience and/or test data. The most widely cited reference is that of Carucci and Mueller (see [10], and [11]) for steel pipe.

Figure 2 illustrates the failure criteria developed originally by Carucci and Mueller and later modified by Eisinger. This failure criteria establishes a design sound power level vs. the ratio of pipe diameter to thickness. This criteria is fundamentally better than the other criteria based on pipe diameter only since thicker wall pipes are stronger than thinner wall pipes.

The original work by Carucci and Mueller suggests a limit provided by the following equation (Figure 2):

$$L_{W,limit} = 184.6 - 0.215\frac{2D_i}{D_o - D_i} = 184.6 - 0.215\frac{D_i}{\delta} \tag{35}$$

where δ is the pipe thickness.

The lower allowable limit developed by Eisinger also shown Figure 2 is given by the following equation:

$$L_{W,limit} = 173.6 - 0.125\frac{2D_i}{D_o - D_i} = 173.6 - 0.125\frac{D_i}{\delta} \tag{36}$$

The NORSOK standard published guidance in 2006 using the same equation for $L_{W,limit}$ as proposed by Eisinger above.

Note that the above limits are based on sound power levels calculated using the source pressure and the downstream exit pressure. We have recalculated the sound power levels based on the correct pressure ratios downstream of the choke point. This data is shown in Figures 3, 4, and 5.

Another design limit criterion that was originally proposed by Carucci and Mueller is based on pipe diameter only for steel pipe. This criterion applies to pipe diameters ranging from 10 inch to 36 inch (approximately between 200 mm to 800 mm) and with wall thicknesses ranging from 0.219 in to 0.439 in (approximately 5.5 mm to 10 mm). The design limit is shown in Figure 3 for the corrected data and can be approximated by:

$$L_{W,limit} = 192.8 - 9.8 \ln D \tag{37}$$

where D is the nominal pipe diameter in inches and L_W is the sound power limit in dB.

The design limit correlations developed in this paper can be used with computer programs such as SuperChems Expert which calculates the sound power level at every axial locations for single and multiphase flow to decide if the steel piping inside diameter to thickness ratio exceed the allowable limits as shown by Figure 6.

Figure 2: Piping failure limit as originally proposed by Carucci and Mueller and by Eisinger for steel pipe

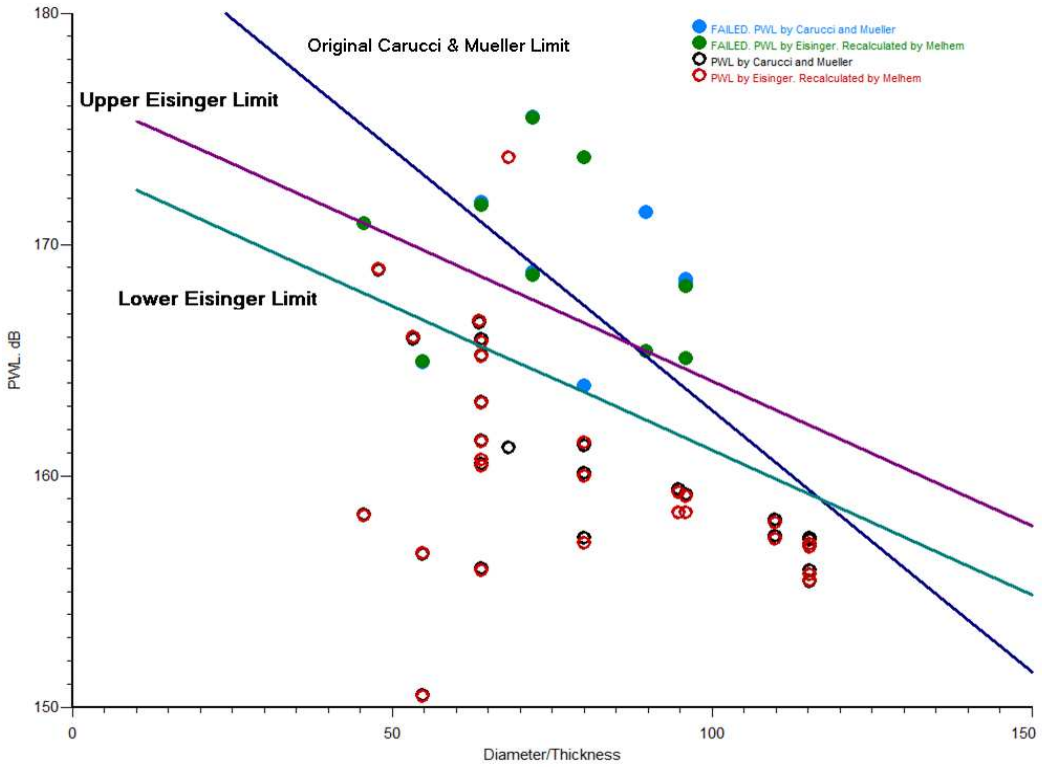

11 Other Methods for Calculating η

The simplest method for calculating η is to assume the same efficiency as an expanded jet (see Figure 7) and apply it equally to single and multi-phase flow. The efficiency shown in Figure 7 is the same as is currently used by API for the estimation of flare noise.

The efficiency is related to the flow pressure ratio and the flow regime as well. IEC calculates the efficiency based on five different flow regimes (see Figure 8) depending on the value of the downstream pressure, P_2:

Regime I The flow is sub-sonic. The sound generation has the character of a dipole jet. The highest Mach number is reached at the vena contracta, not exceeding Mach 1 at the maximum. Downstream of the vena contracta, the jet expands, leading to partial pressure recovery (F_L factor).

Regime II Sonic and supersonic flows exist together, which means that strongly turbulent flow and shock cell structure dominate. Pressure recovery drops until the top limit of regime II is reached.

Regime III The rise in pressure is non-isentropic. The flow is supersonic and shear turbulence predominates.

Figure 3: Piping failure correlation developed by Melhem using Carucci Mueller acoustic efficiency and corrected sound power level estimates for steel pipe. PWL vs. D

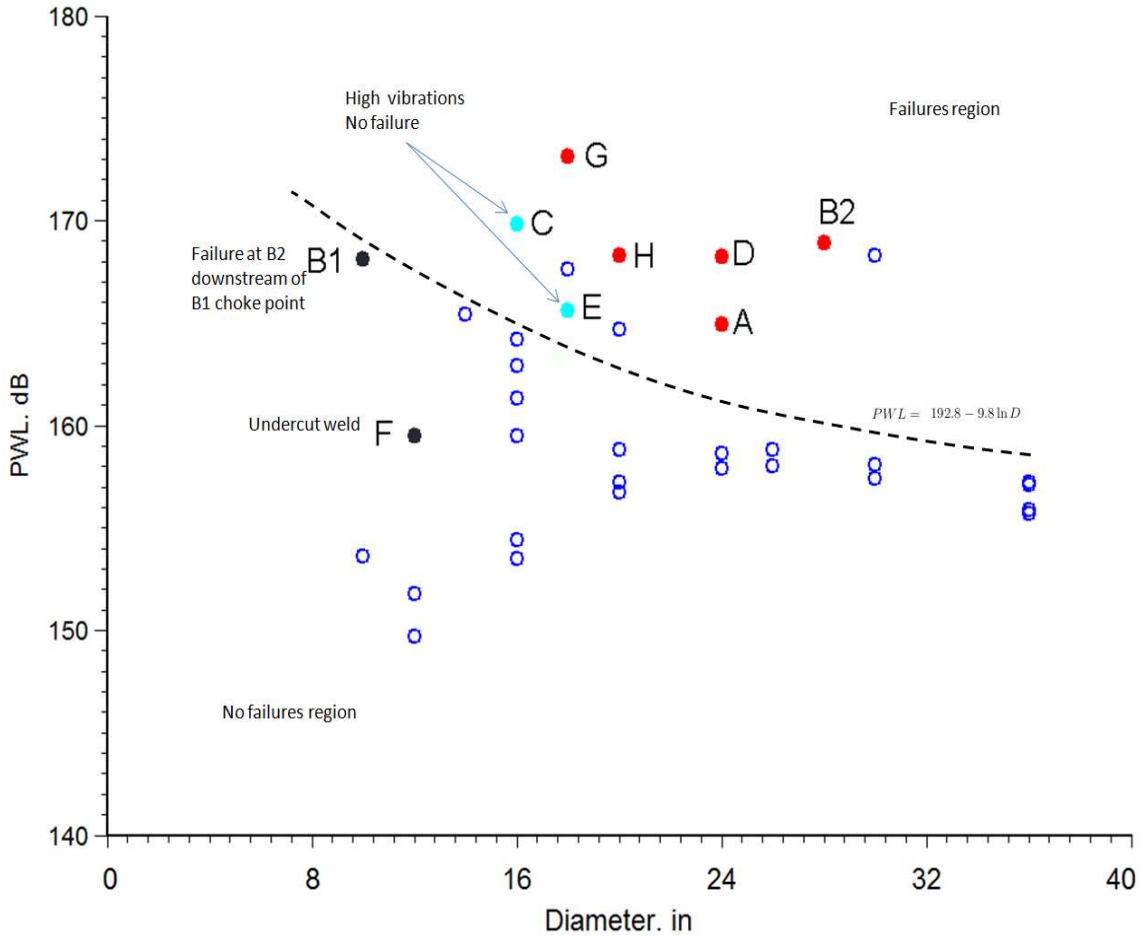

Regime IV The shock cells disappear and a Mach disk forms. The dominant mechanism is the interaction between shock cells and turbulence.

Regime V The acoustical efficiency is constant.

The flow regime types are defined by varying jet shapes in the area upstream and downstream of the vena contracta. These jets change their shape when certain differential pressure ratios are exceeded. In regimes II to IV, higher Mach numbers arise downstream of the vena contracta. Yet, M at the vena contracta itself remains unchanged at 1. The IEC method produces equivalent values of efficiency to the data shown in Figure 7 (as $F_L \rightarrow 1.0$) as shown in Figure 9. Note that Figure 9 uses $x = 1 - P_2/P_1$ as the X axis while Figure 7 uses $P_1/P_2 = \frac{1}{1-x}$.

Figure 4: Piping failure correlation developed by Melhem using Carucci Mueller acoustic efficiency and corrected sound power level estimates for steel pipe. PWL vs. D/t

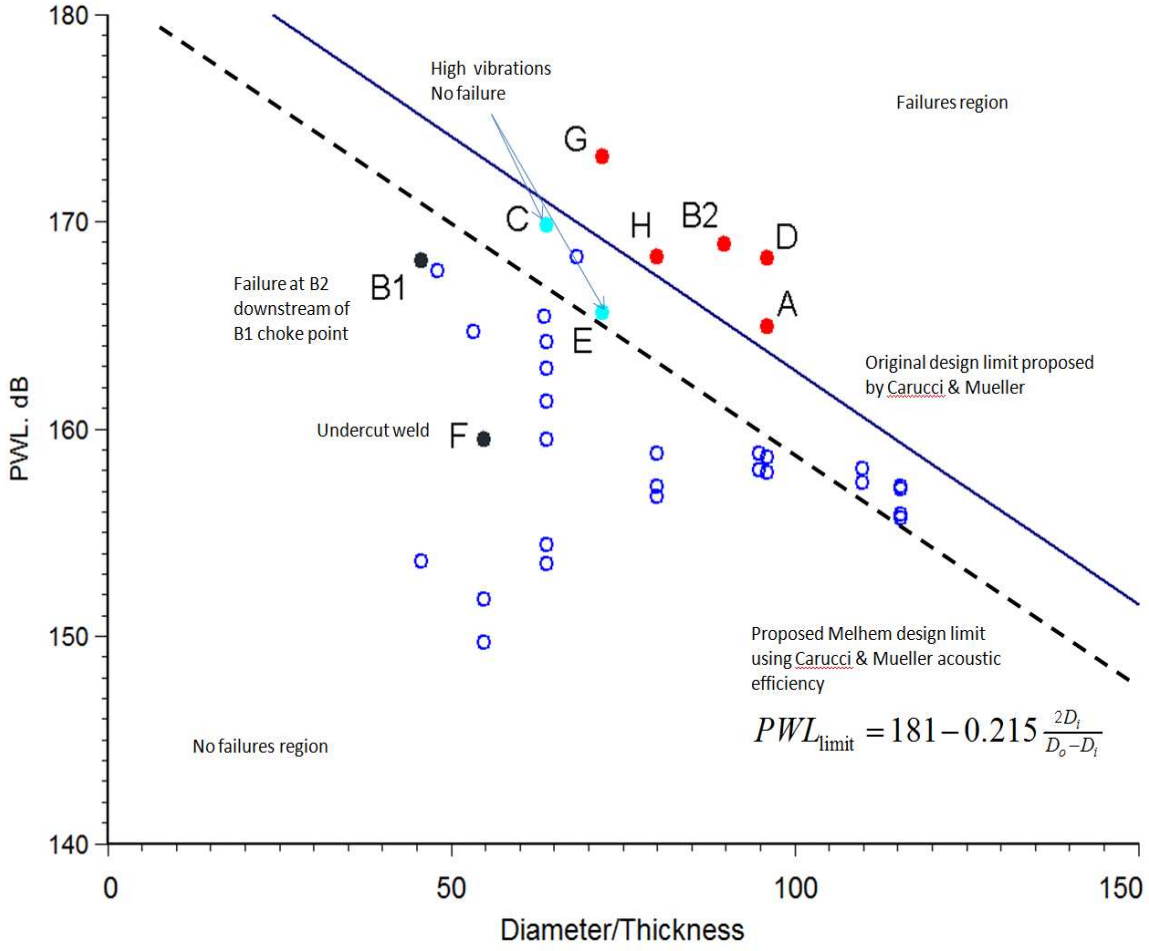

12 Vibration Frequencies

As a fluid moves through piping components there likely will be a separation of the fluid from the constraining wall as the fluid changes flow direction. As a result a vortex is formed and then swept into the main stream. This vortex shedding occurs at fairly well defined dimensionless frequencies. The strength of the vortex varies but does not need to be very strong to cause damage especially if the shedding frequency couples with the natural frequency of the piping system. The shedding peak frequency for a vortex for subsonic and sonic flows (regimes I and II up to a Mach number of 1.4) is given by:

$$f_p = \frac{N_{Str} u}{D} = 0.2 \frac{u}{D} \tag{38}$$

where u is the flow velocity in $\mathrm{m/s}$, D is a characteristic flow dimension (perpendicular to flow), f_p is the peak frequency in Hz and N_{Str} is the Strouhal Number which varies depending upon the

Figure 5: Piping failure correlation developed by Melhem using IEC acoustic efficiency and corrected sound power level estimates for steel pipe. PWL vs. D/t

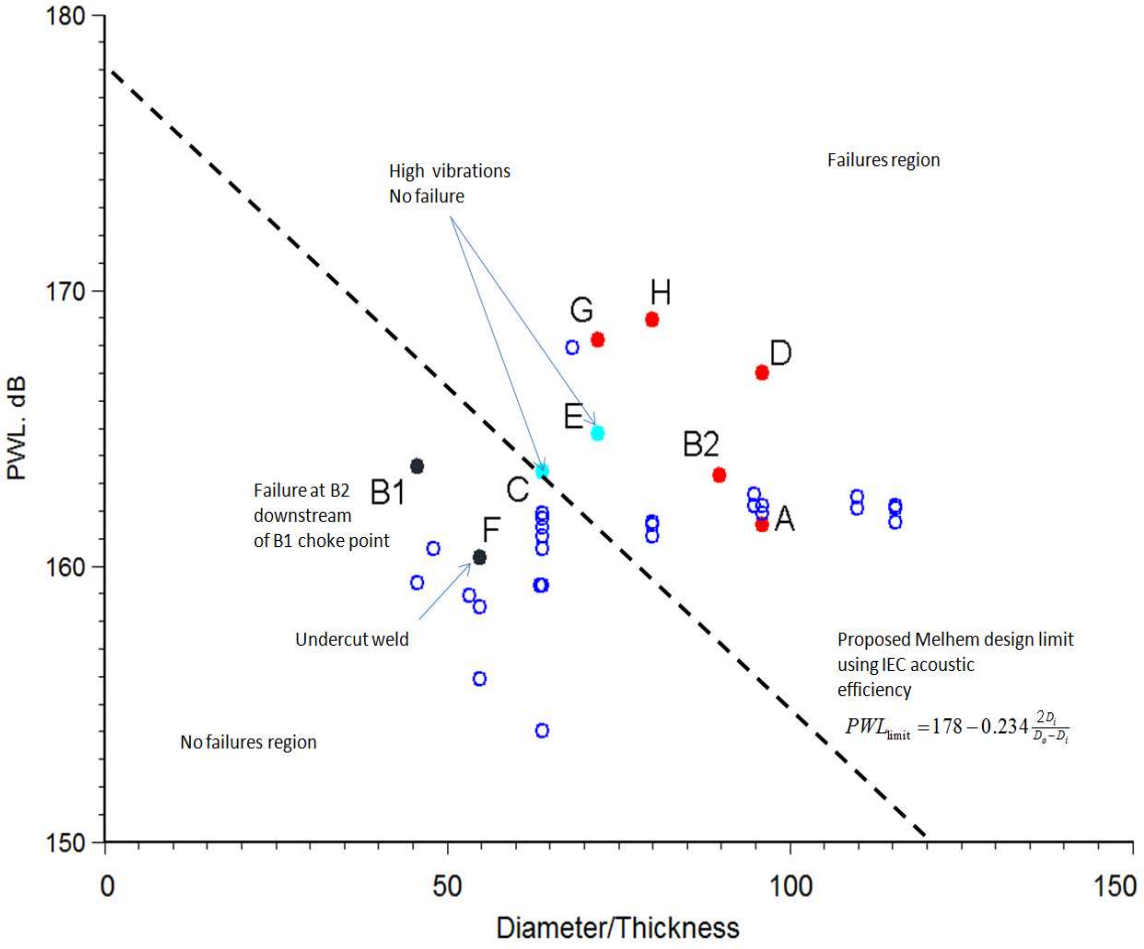

geometry causing the separation of the boundary layer. For a circular cylinder its value is 0.2 over a wide range of Reynolds numbers. It is usually between 0.1 and 0.3. Vortex shedding frequencies are generally more than 30 Hz [upper limit for most piping system natural frequencies].

For flows with Mach numbers larger than 1.4 ($M > 1.4$, regimes III to V), the peak frequency $f_p$is given by:

$$f_p = \frac{0.4 u_{sonic}}{1.25 D \sqrt{M^2 - 1}} \tag{39}$$

For pipe flow, D is equal to the inside flow diameter. For a control valve, D is given by:

$$D = 0.0046 \sqrt{\frac{C_v F_l}{N_o}} \tag{40}$$

where D is in meters, N_o is the number of separate flow passages, C_v is the valve flow coefficient, $\frac{C_v}{N_o}$ is the channel flow coefficient, and F_l is the valve recovery factor. The pressure recovery factor

Figure 6: Sample piping sound power level calculated by SuperChems Expert v6.4mp vs. experience based allowable limit for steel pipe

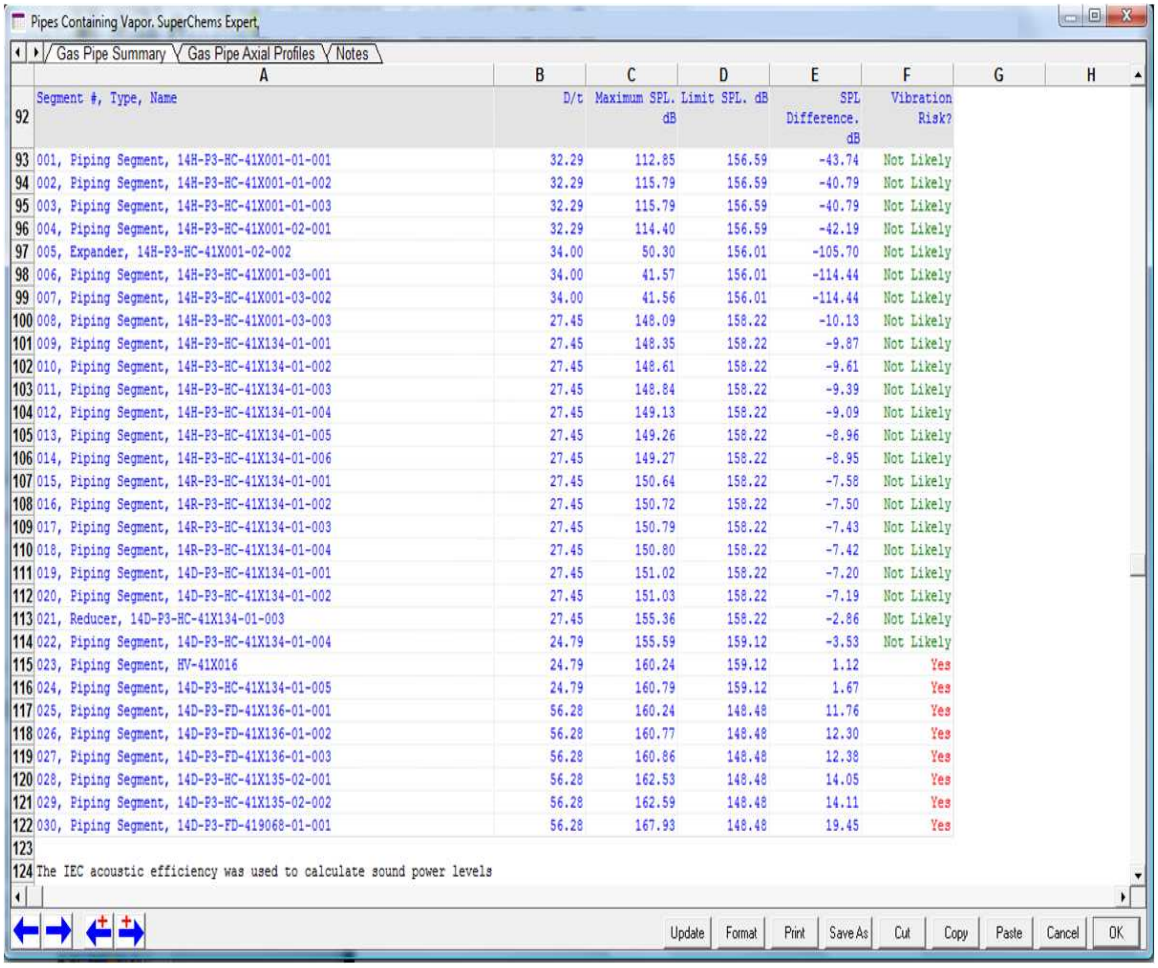

Pipes Containing Vapor. SuperChems Expert.

Gas Pipe Summary | Gas Pipe Axial Profiles | Notes

	A	B	C	D	E	F	G	H
92	Segment #, Type, Name	D/t	Maximum SPL. dB	Limit SPL. dB	SPL Difference. dB	Vibration Risk?		
93	001, Piping Segment, 14H-P3-HC-41X001-01-001	32.29	112.85	156.59	-43.74	Not Likely		
94	002, Piping Segment, 14H-P3-HC-41X001-01-002	32.29	115.79	156.59	-40.79	Not Likely		
95	003, Piping Segment, 14H-P3-HC-41X001-01-003	32.29	115.79	156.59	-40.79	Not Likely		
96	004, Piping Segment, 14H-P3-HC-41X001-02-001	32.29	114.40	156.59	-42.19	Not Likely		
97	005, Expander, 14H-P3-HC-41X001-02-002	34.00	50.30	156.01	-105.70	Not Likely		
98	006, Piping Segment, 14H-P3-HC-41X001-03-001	34.00	41.57	156.01	-114.44	Not Likely		
99	007, Piping Segment, 14H-P3-HC-41X001-03-002	34.00	41.56	156.01	-114.44	Not Likely		
100	008, Piping Segment, 14H-P3-HC-41X001-03-003	27.45	148.09	158.22	-10.13	Not Likely		
101	009, Piping Segment, 14H-P3-HC-41X134-01-001	27.45	148.35	158.22	-9.87	Not Likely		
102	010, Piping Segment, 14H-P3-HC-41X134-01-002	27.45	148.61	158.22	-9.61	Not Likely		
103	011, Piping Segment, 14H-P3-HC-41X134-01-003	27.45	148.84	158.22	-9.39	Not Likely		
104	012, Piping Segment, 14H-P3-HC-41X134-01-004	27.45	149.13	158.22	-9.09	Not Likely		
105	013, Piping Segment, 14H-P3-HC-41X134-01-005	27.45	149.26	158.22	-8.96	Not Likely		
106	014, Piping Segment, 14H-P3-HC-41X134-01-006	27.45	149.27	158.22	-8.95	Not Likely		
107	015, Piping Segment, 14R-P3-HC-41X134-01-001	27.45	150.64	158.22	-7.58	Not Likely		
108	016, Piping Segment, 14R-P3-HC-41X134-01-002	27.45	150.72	158.22	-7.50	Not Likely		
109	017, Piping Segment, 14R-P3-HC-41X134-01-003	27.45	150.79	158.22	-7.43	Not Likely		
110	018, Piping Segment, 14R-P3-HC-41X134-01-004	27.45	150.80	158.22	-7.42	Not Likely		
111	019, Piping Segment, 14D-P3-HC-41X134-01-001	27.45	151.02	158.22	-7.20	Not Likely		
112	020, Piping Segment, 14D-P3-HC-41X134-01-002	27.45	151.03	158.22	-7.19	Not Likely		
113	021, Reducer, 14D-P3-HC-41X134-01-003	27.45	155.36	158.22	-2.86	Not Likely		
114	022, Piping Segment, 14D-P3-HC-41X134-01-004	24.79	155.59	159.12	-3.53	Not Likely		
115	023, Piping Segment, HV-41X016	24.79	160.24	159.12	1.12	Yes		
116	024, Piping Segment, 14D-P3-HC-41X134-01-005	24.79	160.79	159.12	1.67	Yes		
117	025, Piping Segment, 14D-P3-FD-41X136-01-001	56.28	160.24	148.48	11.76	Yes		
118	026, Piping Segment, 14D-P3-FD-41X136-01-002	56.28	160.77	148.48	12.30	Yes		
119	027, Piping Segment, 14D-P3-FD-41X136-01-003	56.28	160.86	148.48	12.38	Yes		
120	028, Piping Segment, 14D-P3-HC-41X135-02-001	56.28	162.53	148.48	14.05	Yes		
121	029, Piping Segment, 14D-P3-HC-41X135-02-002	56.28	162.59	148.48	14.11	Yes		
122	030, Piping Segment, 14D-P3-FD-419068-01-001	56.28	167.93	148.48	19.45	Yes		
123								
124	The IEC acoustic efficiency was used to calculate sound power levels							

Update | Format | Print | Save As | Cut | Copy | Paste | Cancel | OK

is defined as:

$$F_l = \sqrt{\frac{P_1 - P_2}{P_1 - P_{vc}}} \tag{41}$$

where $P_1 - P_2$ is the pressure differential across the valve and P_{vc} is the pressure at the vena contracta (note that P_2 is larger than P_{vc} since the pressure at the exit of the valve recovers):

$$P_{vc} = P_1 - \frac{P_1 - P_2}{F_l^2} \tag{42}$$

For liquid flow, P_{vc} can reach the vapor pressure of the liquid and cause choked flow.

$$P_{vc} = F_f P_v \simeq \left[0.96 - 0.25\sqrt{\frac{P_v}{P_c}}\right] P_v \tag{43}$$

Figure 7: Acoustic efficiency of shock noise generated by choked jets, η vs. jet pressure ratio P_1/P_2 [1]

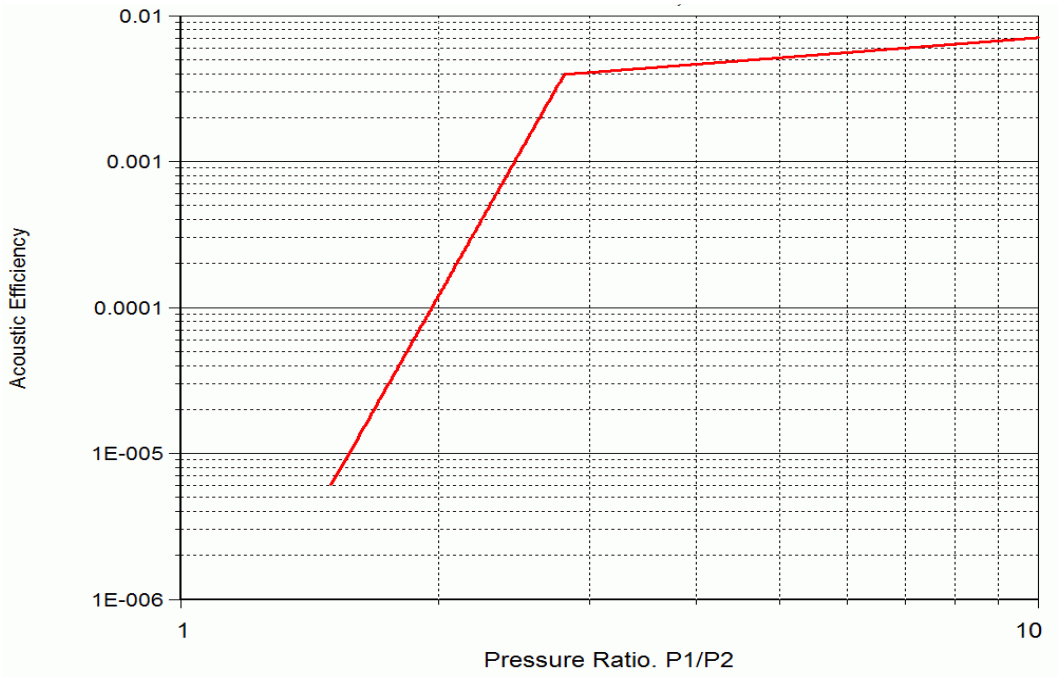

where F_f is the liquid critical pressure factor, P_v is the liquid vapor pressure, and P_c is the liquid critical pressure.

The lowest possible value of P_{vc} in a valve flowing liquid, would be vacuum or 0. For this particular limiting case, Equation 41 can be solved for the pressure ratio P_1/P_2:

$$P_d = \frac{P_1}{P_2} = \frac{1}{1 - F_l^2} \tag{44}$$

where P_d is the damaging pressure ratio. If the valve is operated at a pressure ratio exceeding P_d, the flow will be choked, noisy, and subject to excessive vibration. Table 2 shows typical valve values for F_l and P_d.

Within every flowing pipe there will also be a standing wave moving axially back and forth in the pipe. The frequency of this wave depends on the effective acoustic length of the pipe and the sonic velocity of the fluid in the pipe. The effective acoustic length of the pipe is the distance between obstructions or acoustic barriers. Examples of obstructions would be valves, pumps, and orifices. An acoustic barrier would be an opening into a larger pipe, a reservoir, the end of a pipe run such as a T intersection where the branch of interest requires a right angle turn. Piping components such as expanders or reducers could be an obstruction. Any analysis should look at the frequencies with and without the expanders as obstructions.

The frequency of the standing wave can be calculated as shown below and then compared to the natural frequencies of valve components and the piping system to determine if there is a potential for vibration and/or resonance.

Figure 8: Flow regimes considered for the estimation of acoustical efficiency

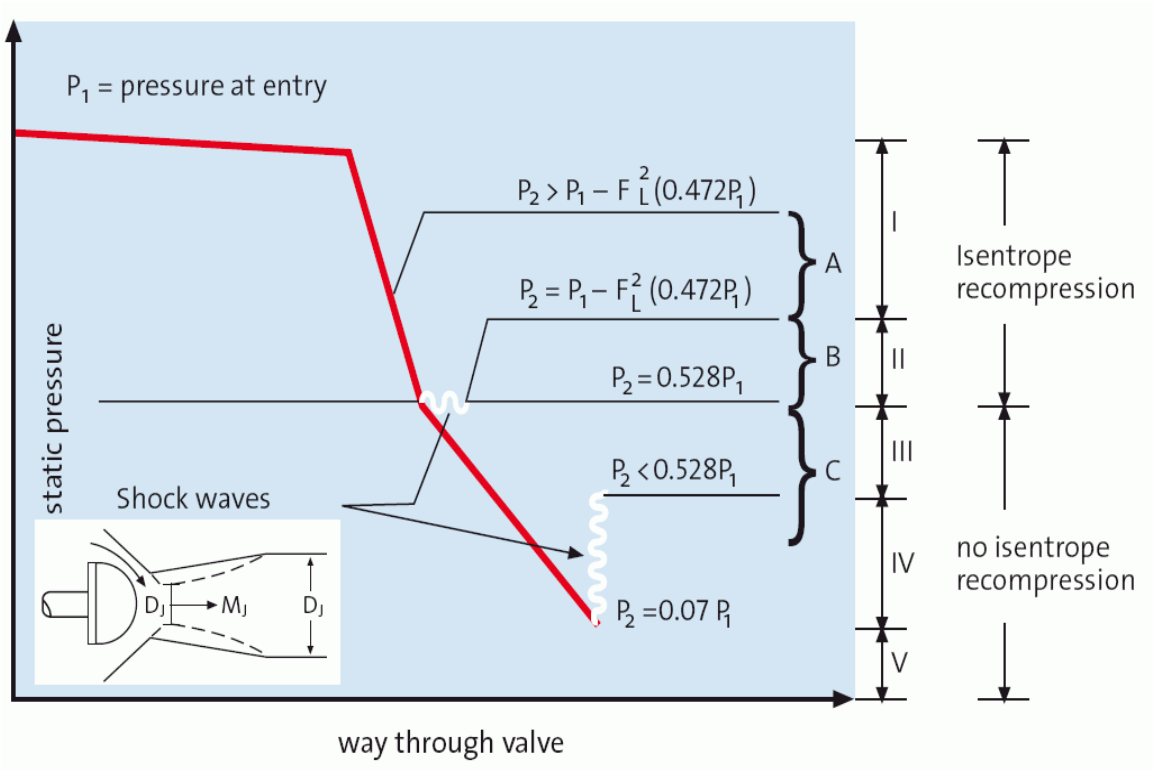

Closed End Pipe $f = \frac{i*u_{ac}}{4L}$

Open End Pipe $f = \frac{i*u_{ac}}{2L}$

where $i = 1, 2, ...$ is the wave number, L is the length between acoustic barriers, and u_{ac} is a characteristic acoustic speed throughout the pipe contents defined as follows:

$$u_{ac} = \frac{u_{sonic}}{\sqrt{1 + \frac{dK}{\delta E}}} \tag{45}$$

where u_{sonic} is the speed of sound in the fluid, K is the bulk modulus of elasticity in the fluid, d is the pipe diameter, δ is the pipe thickness and E is the pipe material of construction modulus of elasticity.

The above equation is derived from a more general form that depends on the elastic properties of the pipe:

$$u_{ac} = \frac{u_{sonic}}{\sqrt{1 + \frac{K}{E}\psi}} \tag{46}$$

where ψ is a function of the elastic properties of the pipe. Typical expressions of ψ are shown in Table 4. Typical material properties for ψ are shown in Table 3. Note that materials properties

Figure 9: IEC Flow Acoustical Efficiency as a Function of F_L and Differential Pressure Ratio

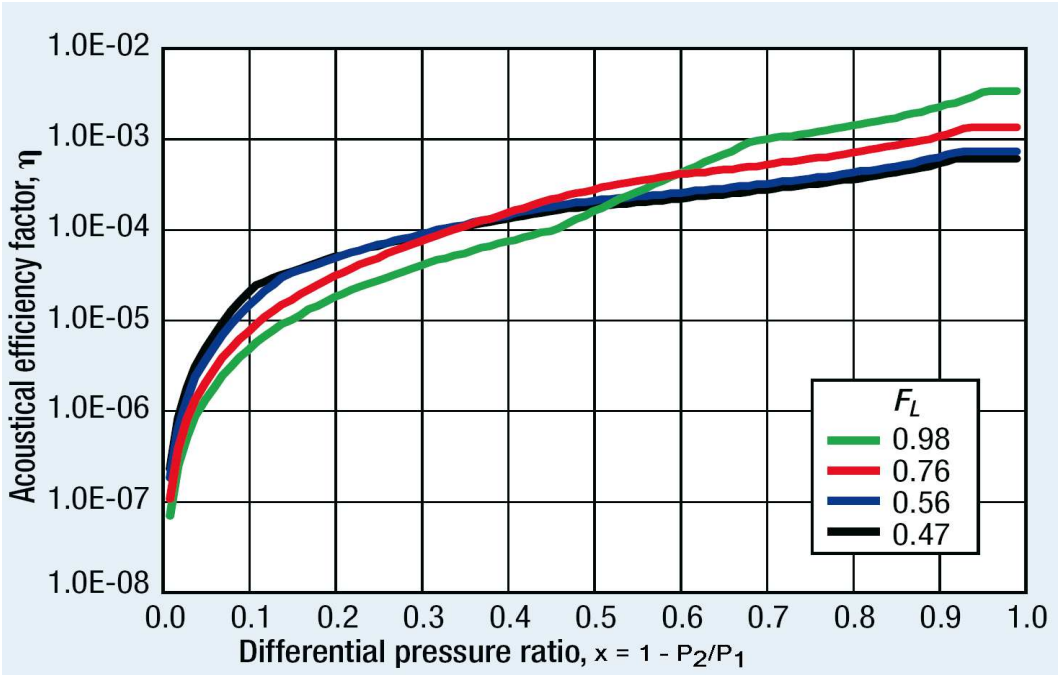

change with temperature as shown in Figure 10 The speed of sound will change as a function of pressure, temperature, and composition. The presence of dissolved gas nuclei (such as air or other gases) in compressed liquids can significantly reduce the sonic velocity following a pressure drop which leads to the formation of gas bubbles. Up to 40 % reduction in sonic velocity has been observed (see Streeter and Wylie [12]).

To control the vibration caused by a standing wave it is necessary to change the magnitude and/or the frequency of the standing wave or to change the natural frequency of the pipe or components being excited by the wave. The best approach is to address the magnitude of the standing wave. The magnitude is related to the fluid turbulent energy that is enforcing the wave. The most dominant source of this turbulence is the kinetic energy generated by the fluid jet exiting the valve trim. Thus a valve change with a trim that reduces this jet energy will eliminate this wave influence. Trying to change the frequencies is usually not beneficial. There is such a wide range of frequencies present in the turbulent flow that excitation can continue to establish a strong wave at the new frequency and continue the piping vibration.

13 The Singing Safety Relief Valve Problem

As a result of increasing steam flow rates, several boiling water reactor (BWR) nuclear power plants have recently experienced the excitation of acoustic standing waves in closed side branches, e.g., safety relief valves (SRVs), due to vortex shedding generated by steam flow in the main steam lines (see Figure 11). Flow past a valve entrance cavity excites a standing wave, resulting in noise and vibration [13]. A similar tone is produced when air is blown across the mouth of a glass bottle.

Table 2: Typical valve values for F_l and P_d

Body	Trim	Flow Direction	F_l	$P_d = \frac{P_1}{P_2}$
Single Seat Globe	Cage	Open	0.90	5.3
	Cage	Closed	0.80	2.8
	V Plug	Open	0.90	5.3
	V Plug	Closed	0.90	5.3
	Contoured	Open	0.90	5.3
	Contoured	Closed	0.80	2.8
Double Seat Globe	V Plug		0.90	5.3
	Contoured		0.85	3.6
	Standard Bore		0.55	1.4
	Characterized		0.57	1.5
Angle	Cage	Open	0.85	3.6
	Cage	Closed	0.80	2.8
Ball	0.8 dia. Orifice		0.55	1.4
Butterfly	60°	Open	0.68	1.8
Butterfly	90°	Open	0.55	1.4

The amplitude of the acoustic pressure waves can be several times higher than the dynamic pressure present in the system (see Figure 12). The acoustic waves propagate in the steam lines, eventually reaching sensitive components such as steam dryers and turbine stop valves. In addition, the acoustic waves generated in the side branches may generate vibration problems locally and may lead to complications such as valve-seat wear. Therefore, the structural components are subjected to high-cycle fatigue loads, which over time may severely impact those components functionality and safety.

Resonance occurs when the vortex shedding frequency coincides with the acoustic frequency of the standpipe or the valve components. The natural frequency of the standpipe/valve combination for a closed end pipe is given by the following equation:

$$f_a = \left(\frac{2n-1}{4}\right)\frac{u_{ac}}{L+L_e} = \left(\frac{2n-1}{4}\right)\frac{u_{ac}}{L+0.425d} \tag{47}$$

where n is the mode number (1 for 1st mode, 2 for 3rd mode, etc.), u_{ac} is the acoustic speed through the pipe contents as defined earlier, and L_e is an end correction corresponding to Rayleigh's upper limit.

The frequency of pressure oscillations (sound) created by vortex shedding, the energy source for the standing waves, is given by the following equation:

$$f_s = N_{str}\frac{u}{d+r} \simeq 0.33\,(n-0.25)\,\frac{u}{d+r} \tag{48}$$

Typically peak oscillations occur at a Strouhal Number around 0.4 as shown in Figure 12. Note that the root mean square pressure amplitude shown in Figure 12 is the ratio of pressure oscillations

Figure 10: Temperature effects on material of construction

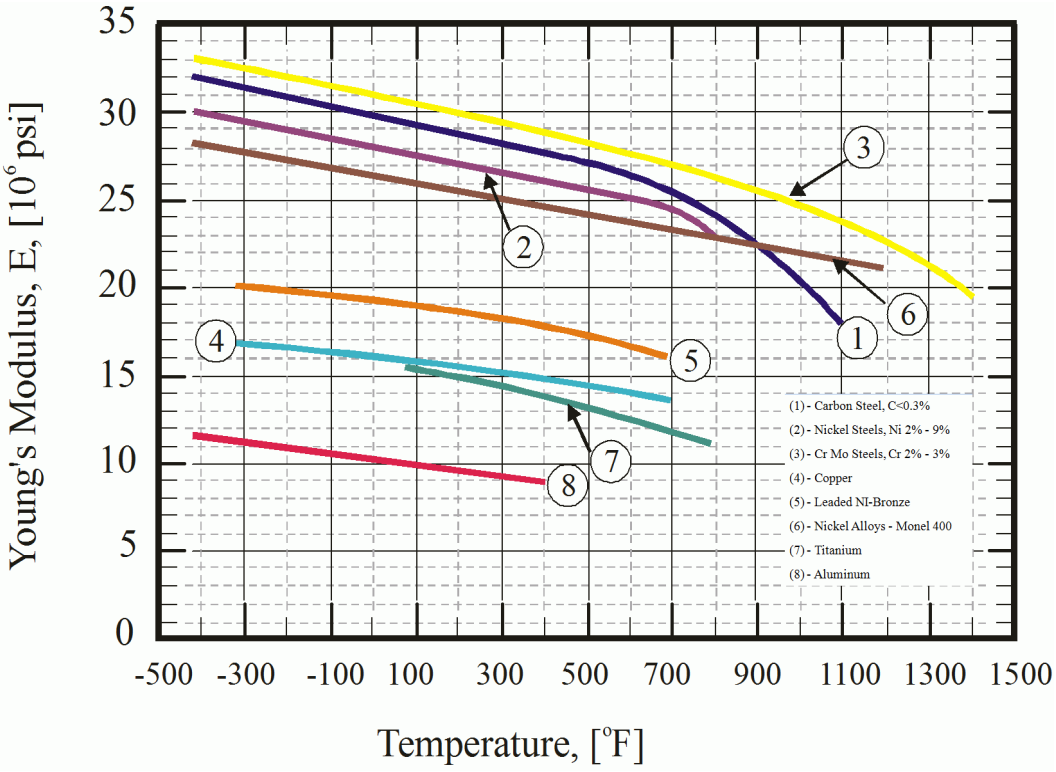

divided by dynamic pressure ($\frac{1}{2}\rho u^2$). RMS begins increasing at a specific onset Strouhal Number and flow velocity depending on acoustic speed, pipe diameter, and pipe length, reaches a peak value and then decreases.

There are many similar installations of pressure relief valves in the process industries where the valves are mounted on large process lines such as overhead lines for distillation columns. In order to avoid fatigue failure from resonance caused by the coupling of normal flow vortex shedding frequency and the acoustic frequency of the standpipe ($f_s = f_a$), the normal flow velocity in the main line has to be limited to less than this critical value:

$$\begin{aligned} u_{max} &< \frac{f_s}{N_{st}}(d+r) < \frac{1}{4}\left(\frac{u_{ac}}{L+L_e}\right)\left(\frac{d+r}{N_{str}}\right) \\ &< \frac{1}{4}\left(\frac{u_{ac}}{L+0.425d}\right)\left(\frac{d+r}{0.6}\right) \end{aligned} \tag{49}$$

As shown in Figure 12 the pressure fluctuations start to increase at a Strouhal number of 0.6 and then decrease after they reach a peak value around a Strouhal number of 0.4.

The same approach can be applied to the flow through the inlet and/or discharge line of a pressure relief valve:

$$u_{max} < \frac{1}{2}\frac{u_{ac}}{L}\frac{D}{0.6} \tag{50}$$

Figure 11: The Singing Safety Relief Valve [2]

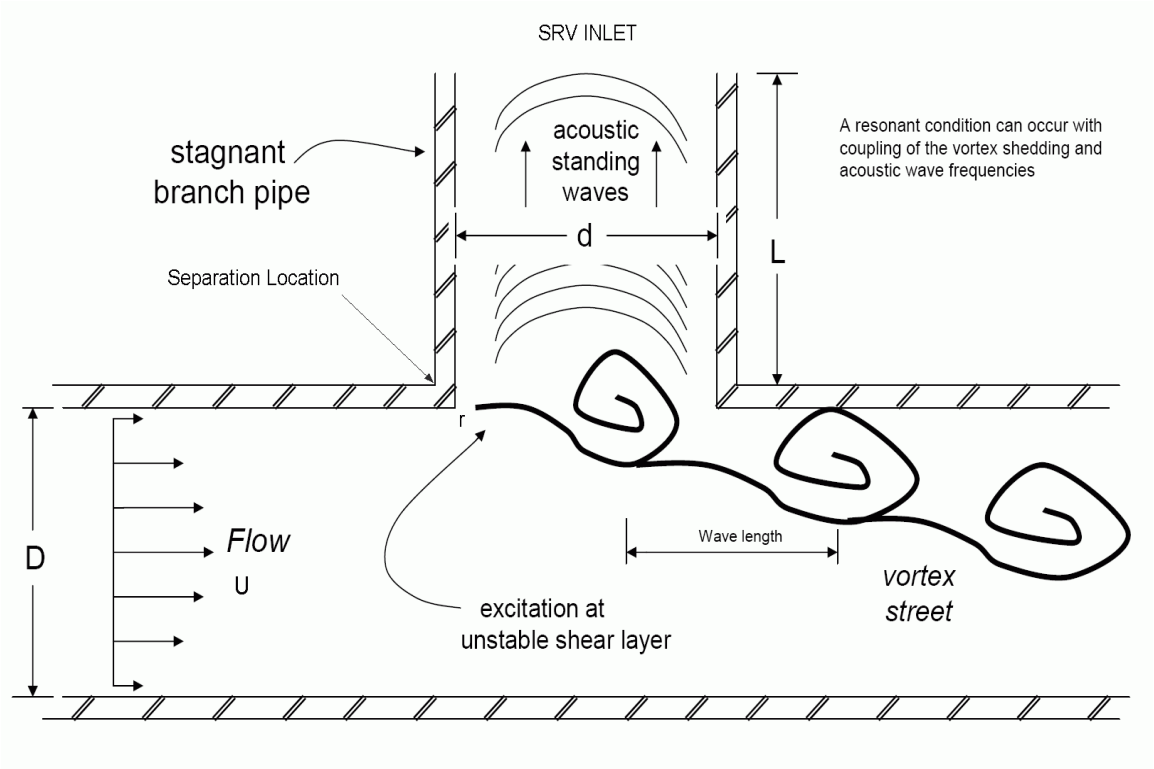

Figure 12: Comparison of Calculated and Measured Pressure Fluctuations as a Function of Strouhal Number [3]

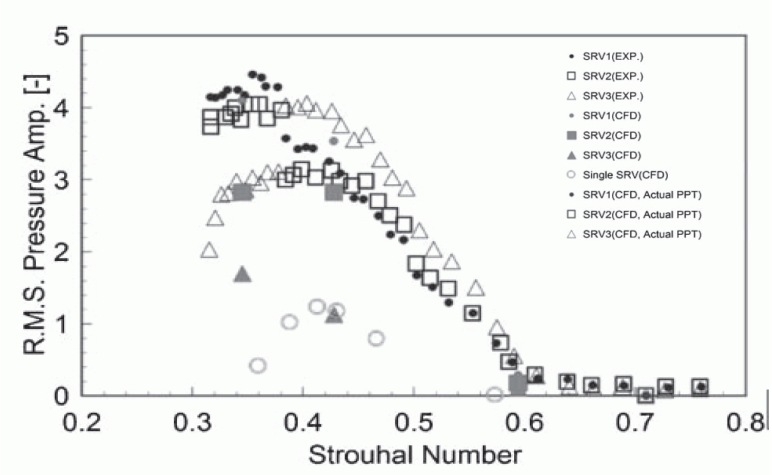

Table 3: Typical data used in the estimation of sonic velocity in pipelines

Material	E (GPa)	Poisson's Ratio ν	$K = \frac{1}{\kappa}$ (GPa)	ρ in $\mathrm{kg/m3}$
Aluminum	69	0.33		
Brass	78-110	0.36		
Carbon steel	202	0.303		
Cast iron	90-160	0.25		
Concrete	20-30	0.15		
Copper	117	0.36		
Ductile iron	172	0.30		
Fibre cement	24	0.17		
High carbon steel	210	0.295		
Inconel	214	0.29		
Mild steel	200-212	0.27		
Nickel steel	213	0.31		
Plastic / Perspex	6.0	0.33		
Plastic / Polyethylene	0.8	0.46		
Plastic / PVC rigid	2.4-2.75			
Stainless steel 18-8	201	0.30		
Water - fresh			2.19	999 at 20 C
Water - sea			2.27	1025 at 15 C

E is typically referred to as Young's modulus of elasticity
G is typically referred to as modulus of torsion, $G = \frac{1}{2}\frac{E}{1+\nu}$

where L is the acoustic length of the inlet or discharge line. Resonance can also be checked by comparing an open pipe/contents frequency with the natural frequency of the pressure relief valve, f_n:

$$f_n = \frac{1}{\tau_n} = \frac{\omega_n}{2\pi} = \frac{1}{2\pi}\sqrt{\frac{K_s}{m_D}} \tag{51}$$

$$\tau_n = \frac{2\pi}{\omega_n} = 2\pi\sqrt{\frac{m_D}{K_s}} \tag{52}$$

where τ_n is the undamped natural period in s, and f_n is the undamped natural frequency in Hz where one Hz equals 1 cycle/second, K_s is the spring constant in $\mathrm{N/m}$, m_D is the mass of the valve disc and moving parts in kg, and ω_n is the undamped circular natural frequency in $\mathrm{radians/s}$.

Table 4: Typical expressions for ψ

Pipe condition	ψ
Rigid	0
Anchored against longitudinal movement through its length	$\frac{d}{\delta}(1-\nu^2)$
Anchored against longitudinal movement at the upper end	$\frac{d}{\delta}(1.25-\nu)$
Frequent expansion joints present	$\frac{d}{\delta}$

14 Conclusions

This papers demonstrates that the Carucci and Mueller equation can produce unrealistic values of acoustic efficiency, well in excess of 1 percent for high pressure systems and/or systems with large mechanical flow energy. Thus, it is recommended that the Carucci and Mueller acoustic efficiency value be limited to a maximum of 2 percent if the calculated value exceeds 2 percent. The revised experience based failure criteria by Melhem (see Figure 5) based on the IEC acoustic efficiency is now recommended for single and multiphase flow.

The piping vibration risk assessment tools incorporated in SuperChems Expert are versatile and incorporate the methods outlined by the Energy Institute and those originally proposed by Carucci and Mueller. However, the SuperChems Expert methods can accurately calculate the absolute value of the sound power level at every axial piping location for single and multiphase flow using a more fundamental representation of sound power level and more realistic acoustic efficiencies. The SuperChems Expert solution can inherently show the impact of using pipe expansions and limiting flow orifice plates for example to reduce the sound power level and to alter the noise peak frequency. The SuperChems Expert implementation is immediately applicable to headers and flare networks where the flow mechanical energy is automatically calculated at the various flow/flare network nodes.

15 Appendix A: Internal Pipe Noise

The flow mechanical energy converted to noise can be related to sound pressure for reflection free planar waves inside the pipe:

$$W = \frac{P^2 A_i}{\rho u_{sonic}} = \frac{\pi D_i^2 P^2}{4 \rho u_{sonic}} \tag{53}$$

where u_{sonic} is the downstream fluid speed of sound, ρ is the downstream fluid density, A_i is the pipe cross sectional flow area, and D_i is the inside pipe diameter. The sound power level can be calculated in decibels refereced to 2×10^{-5} Pascals:

$$L_{P,i} = 10 \log_{10} \left[\frac{P^2}{(2 \times 10^{-5})^2} \right] \tag{54}$$

$L_{P,i}$ can be expressed as a function of W:

$$L_{P,i} = 10 \log_{10} \left[\frac{\rho u_{sonic} W}{\pi D_i^2 10^{-10}} \right] = 10 \log_{10} \left[3.183 \times 10^9 \frac{\rho u_{sonic} W}{D_i^2} \right] \tag{55}$$

The above equation can be used to calculate to the total internal sound pressure assuming 100 % of the noise is transmitted downstream. If the flow exits at an angle, only a portion of the total sound pressure level is transmitted downstream:

$$L_{P,i} = 10 \log_{10} \left[3.183 \times 10^9 \frac{\zeta \rho u_{sonic} W}{D_i^2} \right] \tag{56}$$

The value of ζ is 0.25.

A frequency dependent internal sound pressure level can be calculated as a function of the peak frequency f_p established earlier and a specific center frequency f_i:

$$L_{P,i}(f_i) = L_{P,i} + L_{f,i} = L_{P,i} - c - 10 \log_{10} \left[\left(1 + \left[\frac{f_i}{2 f_p} \right]^2 \right) \left(1 + \left[\frac{f_p}{2 f_i} \right]^4 \right) \right] \tag{57}$$

where the constant c is 7.9 for one-third octave center frequencies and 3 for octave center frequencies. Summing $L_{f,i}$ over the entire frequency spectrum should yield a 0:

$$0 = 10 \log_{10} \Sigma_{i=1}^{n=33} 10^{\frac{L_{f,i}}{10}} \tag{58}$$

Table 5: Weighting factor for one-third octave frequencies

f_i in Hz	$W(f_i)$	f_i in Hz	$W(f_i)$
10	-70.4	500	-3.2
12.5	-63.4	630	-1.9
16	-56.7	800	-0.8
20	-50.5	1000	0
25	-44.7	1250	0.6
31.5	-39.4	1600	1
40	-34.6	2000	1.2
50	-30.2	2500	1.3
63	-26.2	3150	1.2
80	-22.5	4000	1
100	-19.1	5000	0.5
125	-16.1	6300	-1.0
160	-13.4	8000	-1.1
200	-10.9	10000	-2.5
250	-8.6	12500	-4.3
315	-6.6	16000	-6.6
400	-4.8	20000	-9.3

16 Appendix B: External Pipe Noise

The pipe absorbs some of the noise and only a portion of the total internal noise escapes to the atmosphere. The sound pressure level at a specific distance from the outer surface of the pipe is given by the following equation:

$$L_{P,e}(f_i) = L_{P,i}(f_i) + TL(f_i) + W(f_i) - 10\log_{10}\left[\frac{2x + 2\delta + D_i}{D_i + 2\delta}\right] \tag{59}$$

where x is the distance from the outer pipe wall, $TL(f_i)$ is the transmission loss at frequency f_i, $W(f_i)$ is the A-weighting factor (see Table 5) for the one-third octave band center frequency f_i, and $L_{P,i}(f_i)$ was defined earlier.

The total sound pressure level received at a location x away from the wall of the pipe can be calculating by summing all the frequency contributions:

$$L_{P,e} = 10\log_{10}\Sigma_{i=1}^{n=33} 10^{\frac{L_{P,e}(f_i)}{10}} \tag{60}$$

The transmission loss can either be ignored (set to 0) or calculated using the method outline by Kiesbauer and Vnucec in 2008. The tranmission loss depends on pipe wall thickness and the

downstream fluid properties:

$$TL(f_i) = 10\log_{10}\left[7.6\times10^7\left(\frac{u_{sonic}}{\delta f_i}\right)^2\frac{G_x(f_i)}{1+\frac{\rho u_{sonic}}{415G_y(f_i)}}\right] - \Delta TL(D_i) \tag{61}$$

where $\Delta TL(D_i)$ is 0 for $D_i > 0.15$ and 9.7 for $D_i < 0.05$. Otherwise it is give by:

$$\Delta TL(D_i) = \frac{16}{(1000D_i - 46)^{0.36}} \tag{62}$$

The values for G_x and G_y are given below:

$$f_r = \frac{5000}{\pi D_i} \tag{63}$$

$$f_o = \frac{f_r}{4}\frac{u_{sonic}}{343} \tag{64}$$

$$f_g = \frac{\sqrt{3}}{\pi\delta}\frac{343^2}{5000} \tag{65}$$

$$G_x(f_i) = \left(\frac{f_o}{f_r}\right)^{2/3}\left(\frac{f_i}{f_o}\right)^4 \quad \text{for} \quad f_i < f_o \tag{66}$$

$$= 1 \quad \text{for} \quad f_i \geq f_o \ \text{ and } \ f_i \geq f_r \tag{67}$$

$$= \sqrt{\frac{f_i}{f_r}} \quad \text{for} \quad f_i \geq f_o \ \text{ and } \ f_i < f_r \tag{68}$$

$$G_y(f_i) = 1 \quad \text{for} \quad f_i < f_o \ \text{ and } \ f_o \geq f_g \tag{69}$$

$$= \frac{f_o}{f_g} \quad \text{for} \quad f_i < f_o \ \text{ and } \ f_o < f_g \tag{70}$$

$$= 1 \quad \text{for} \quad f_i \geq f_o \ \text{ and } \ f_i \geq f_g \tag{71}$$

$$= \frac{f_i}{f_g} \quad \text{for} \quad f_i \geq f_o \ \text{ and } \ f_i < f_g \tag{72}$$

where f_r is the ring frequency and f_o and f_g are the coincidence pipe frequencies.

References

[1] I. Heitner. How to estimate plant noises. *Hydrocarbon Processing*, 47:67–74, 1968.

[2] P. Sekerak. Potential adverse flow effects at nuclear power plants. In *16th International Conference on Nuclear Engineering*. ICONE16-48900, 2008.

[3] K. Okuyama F. Inada Y. Ogawa R. Morita, S. Takahashi and K. Yoshikawa. Evaluation of acoustic and flow induced vibration of the bwr main steam lines and dryer. *Journal of NUCLEAR SCIENCE and TECHNOLOGY*, 48(5):759–776, 2011.

[4] W. A. Skipwith. Acoustics technology. Survey SP-5093, NASA National Aeronautics and Space Administration, 1970.

[5] C. M. Harris. *Handbook of Noise Control*. cGraw-Hill Book Co., Inc., 1957.

[6] N. R. Miller G. M. Singh, E. Rodarte and P. S. Hrnjak. Modification of a standard aeroacoustic valve noise model to account for friction and two-phase flow. In *ACRC TR-162*, pages 1–11. Mechanical and Industrial Engineering Department, University of Illinois, 2000.

[7] N. R. Miller G. M. Singh, E. Rodarte and P. S. Hrnjak. Prediction of noise generated by expansion devices throttling refrigerant. In *ACRC TR-163*, pages 1–13. Mechanical and Industrial Engineering Department, University of Illinois, 2000.

[8] MTD. *Guidelines for the Avoidance of Vibration Induced Fatigue in Process Pipework*. Marine Technology Directorate Limited (MTD), 1999.

[9] Energy Institute. *Guidelines for the Avoidance of Vibration Induced Fatigue in Process Pipework*. The Energy Institute, London, England, 2008.

[10] V. A. Carucci and R. T. Mueller. Acoustically induced piping vibration in high capcity pressure reducing systems. In *82-WA/PVP-8*, pages 1–13. American Society of Mechanical Engineers, ASME, 1982.

[11] F. L. Eisinger. Designing piping systems against acoustically-induced structural fatigue. In *PVP-VOL 328, Flow-Induced Vibration*, pages 397–404. American Society of Mechanical Engineers, ASME, 1982.

[12] V. L. Streeter and E. B. Wylie. Water hammer and surge control. *Annual Reviews in Fluid Mechanics*, pages 57–74, 1974.

[13] T. M. Mulcahy S. A. Hambric and V. N. Shah. Flow-induced vibration effects on nuclear power plant components due to main steam line valve singing. In *Ninth NRC/ASME Symposium on Valves, Pumps, and Inservice Testing, NUREG/CP-0152*, volume 6, pages 3B:49–3B:69. NRC/ASME, 2006.